Article

Effective Control of the Optical Bistability of a Three-Level Quantum Emitter near a Nanostructured Plasmonic Metasurface

Hamid R. Hamedi [1], Emmanuel Paspalakis [2] and Vassilios Yannopapas [3],*

[1] Institute of Theoretical Physics and Astronomy, Vilnius University, Saulėtekio 3, LT-10257 Vilnius, Lithuania; hamid.hamedi@tfai.vu.lt

[2] Materials Science Department, School of Natural Sciences, University of Patras, 265 04 Patras, Greece; paspalak@upatras.gr

[3] Department of Physics, School of Applied Mathematics and Physics, National Technical University of Athens, 157 80 Athens, Greece

* Correspondence: vyannop@mail.ntua.gr

Abstract: We study, theoretically, the phenomena optical bistability and multistability of a hybrid quantum-plasmonic system immersed within an optical ring cavity. The hybrid quantum-plasmonic system consists of a three-level *V*-type quantum emitter and a two-dimensional plasmonic metasurface of gold nanoshells. The quantum emitter and the plasmonic metasurface are placed in close proximity to each other so that a strong quantum interference of spontaneous emission occurs, which enables the strong modification of optical-bistability/ multistability hysteresis curves. Along with this, the strong interaction between the emitter and the plasmonic metasurface allows for active control of the corresponding bistable threshold intensity. Furthermore, we show that by varying the metasurface-emitter separation, a transition from bistability to multistability of the hybrid system is observed. Lastly, by introducing an additional incoherent pumping in the system, we have the emergence of phenomena, such as probe absorption and gain, with or without population inversion. The results may find technological application in on-chip nanoscale photonic devices, optoelectronics and solid-state quantum information science.

Keywords: plasmonic nanospheres; optical bistability; quantum intereference

1. Introduction

Coherent control of light using light is very important in optical computing and all-optical communication. During recent years, optical transistors, all-optical storage and all-optical switching devices based on optical bistability (OB) in two-level atomic configurations have been extensively investigated [1,2]. The OB features in three and multilevel atom-light coupling schemes by means of optical ring cavities were later investigated, both theoretically and experimentally [3–11]. Namely, it was demonstrated that quantum interference effects, such as the electromagnetically induced transparency [12], can be used to significantly decrease the OB threshold.

On the other hand, in recent years, there has been great interest in the nonlinear optical effects of quantum systems in the vicinity of plasmonic nanostructures and metasurfaces. It is known that nonlinear effects in these structures can be significantly modified and even enhanced due to the strong exciton-plasmon coupling for quantum systems near plasmonic nanostructures, the subwavelength concentration of the electric field, as well the significant change of the spontaneous decay rate of the quantum systems due to the plasmonic nanostructures.

Various phenomena have been studied in such media, including the manipulation of spontaneous emission [13–16], Fano effects in energy absorption [17–20], slow light and optical transparency [21–23], enhancement of the refractive index [24], modification and enhancement of the Kerr nonlinearity [25–28], four-wave-mixing [29,30], inversionless

gain [31–36], OB or optical multistability (OM) [37–49], and many others [50–52]. The contemporary fabrication methods [53–56] for realizing plasmonic nanostructures incorporating quantum emitters [57] enable the experimental verification of the above phenomena.

In this work, we consider a closed *V*-type quantum emitter that is placed next to a plasmonic nanostructure, which, altogether, constitutes the *quantum sample*. The quantum sample (emitter+nanostructure) is placed inside a unidirectional optical ring cavity. The focus of the present study is to analyze, theoretically, the phenomenon of OB occurring in the quantum sample placed in this type of cavity.

In particular, we found that the rate of incoherent pumping, the distance of the quantum system from the plasmonic nanostructure, the probe detuning, as well as the doublet splitting dramatically influenced the OB as well as the OM, allowing for a robust manipulation of the corresponding threshold intensity and hysteresis loop. Namely, we demonstrate that by varying the distance of the quantum system from the plasmonic nanostructure, one can achieve a transition from the regime of OB to OM.

The paper is organized as follows: in Section 2, we present the theoretical model and the corresponding formalism. The numerical results and physical analysis are presented in Section 3, while Section 4 concludes the paper.

2. Model and Equations

2.1. Hamiltonian and Master Equations

Figure 1a shows a three-level quantum *V*-type emitter with two closely lying upper states $|2\rangle$ and $|3\rangle$, and a lower state $|1\rangle$. The quantum emitter is surrounded by a vacuum and is placed at a distance d from the surface of a plasmonic metasurface, as illustrated in Figure 1b. The upper states $|2\rangle$ and $|3\rangle$ characterize two Zeeman sublevels ($J = 1$, $M_J = \pm 1$), while the lower state $|1\rangle$ is a corresponding level with $J = 0$. The dipole moment operator is, then,

$$\overrightarrow{\mu} = \mu(|2\rangle\langle 1|\hat{\varepsilon}_- + |3\rangle\langle 1|\hat{\varepsilon}_+) + H.c,\tag{1}$$

where the right-rotating ($\hat{\varepsilon}_+$) and left-rotating ($\hat{\varepsilon}_-$) unit vectors are defined by $\hat{\varepsilon}_\pm = (\mathbf{e}_z + i\mathbf{e}_x)/\sqrt{2}$, while μ is taken to be real.

We assume that the above quantum emitter is illuminated by a linearly polarized electromagnetic plane wave in which case the electric field is $\overrightarrow{E}(t) = \hat{z}E\cos(\omega t)$, where E denotes the electric field amplitude and ω is the angular frequency. The laser field couples the transition between state $|1\rangle$ and states $|2\rangle$ and $|3\rangle$. Under the dipole and rotating-wave approximations, the interaction Hamiltonian describing the light-matter coupling reads

$$H = \hbar\left(-\delta - \frac{\omega_{32}}{2}\right)|2\rangle\langle 2| + \hbar\left(-\delta + \frac{\omega_{32}}{2}\right) - \frac{\hbar\Omega}{2}(|1\rangle\langle 2| + H.c.),\tag{2}$$

where $\delta = \omega - \tilde{\omega}$ is the detuning, $\tilde{\omega} = (\omega_2 + \omega_3)/2 - \omega_0$ and $\omega_{32} = (\omega_3 - \omega_2)/2$. Note that, $\hbar\omega_n$ corresponds to the energy of state $|n\rangle$. The Rabi frequency of the laser field is defined as $\Omega = \mu E\sqrt{2}\hbar$. The excited states $|2\rangle$ and $|3\rangle$ decay spontaneously to state $|1\rangle$ with rates $2\gamma_2$ and $2\gamma_3$, respectively. The frequencies of the transitions from $|2\rangle$, $|3\rangle$ to $|1\rangle$ fall within the band of surface-plasmon excitations of the plasmonic metasurface of nanoshells. Furthermore, two incoherent pump fields r_1 and r_2 ($r_1 = r_2 = r$) are applied as responsible for pumping populations from the lower state $|1\rangle$ to excited states $|2\rangle$ and $|3\rangle$ via a one-way pump process. Γ_0 denotes the free-space decay rate of states $|2\rangle$ and $|3\rangle$ to state $|1\rangle$. Finally, we take that $\gamma_2 = \gamma_3 = \gamma$ [15].
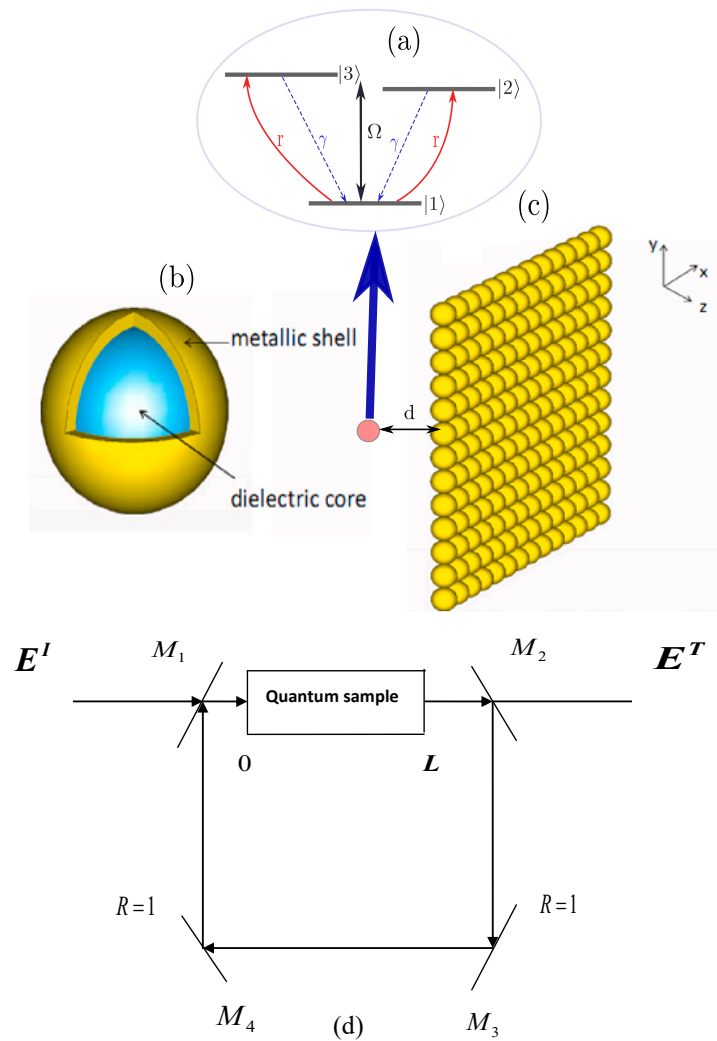
Figure 1. The three-level quantum *V*-system under study (**a**). A silica sphere coated with a gold nanoshell (**b**) and a two-dimensional square lattice of such spheres (**c**). The quantum sample (quantum emitter + array of spheres) is placed inside a unidirectional ring cavity (**d**).

Based on the Markovian approximation and the Hamiltonian of Equation (2), the density-matrix equations of the quantum sample read as

$$\dot{\rho_{21}} = (i\delta + \frac{i\omega_{32}}{2} - \gamma - r)\rho_{21} - i\frac{\Omega}{2}\rho_{22} - i\frac{\Omega}{2}\rho_{23} + i\frac{\Omega}{2}\rho_{11} - \kappa\rho_{31}, \tag{3}$$

$$\dot{\rho_{31}} = (i\delta - \frac{i\omega_{32}}{2} - \gamma - r)\rho_{31} - i\frac{\Omega}{2}\rho_{33} - i\frac{\Omega}{2}\rho_{32} + i\frac{\Omega}{2}\rho_{11} - \kappa\rho_{21}, \tag{4}$$

$$\dot{\rho_{23}} = (i\omega_{32} - 2\gamma)\rho_{23} + i\frac{\Omega}{2}\rho_{13} - i\frac{\Omega}{2}\rho_{21} - \kappa(\rho_{22} + \rho_{33}), \tag{5}$$

$$\dot{\rho_{22}} = -2\gamma\rho_{22} + r\rho_{11} + i\frac{\Omega}{2}(\rho_{12} - \rho_{21}) - \kappa(\rho_{23} + \rho_{32}), \tag{6}$$

$$\dot{\rho_{33}} = -2\gamma\rho_{33} + r\rho_{11} + i\frac{\Omega}{2}(\rho_{13} - \rho_{31}) - \kappa(\rho_{23} + \rho_{32}). \tag{7}$$

The above equations are consistent with the conservation law $\rho_{11} + \rho_{22} + \rho_{33} = 1$ with $\rho_{ij} = \rho_{ji}^*$.

In the above equations, κ corresponds to the coupling coefficient between upper states $|2\rangle$ and $|3\rangle$ resulting from the occurrence of quantum interference of spontaneous emission in an electromagnetically anisotropic environment [58,59].

Here, γ and κ are provided by [13,14,60–64]

$$\gamma = \frac{\mu_0 \mu^2 \bar{\omega}^2}{2\hbar} \hat{\varepsilon}_-.\, Im\mathbf{G}(\mathbf{r},\mathbf{r};\bar{\omega}).\hat{\varepsilon}_+, \tag{8}$$

$$\kappa = \frac{\mu_0 \mu^2 \bar{\omega}^2}{2\hbar} \hat{\varepsilon}_+.\, Im\mathbf{G}(\mathbf{r},\mathbf{r};\bar{\omega}).\hat{\varepsilon}_+, \tag{9}$$

where $\mathbf{G}(\mathbf{r},\mathbf{r};\bar{\omega})$ ($\bar{\omega} = (\omega_3 + \omega_2)/2 - \omega_1$) corresponds to the electromagnetic Green's tensor, $\mathbf{r}$ is the position of the quantum emitter and μ_0 stands for the free-space electric permittivity. Equations (8) and (9) provide the values of γ and κ [13,14,60–64]

$$\gamma = \frac{\mu_0 \mu^2 \bar{\omega}^2}{2\hbar}\, Im\left[G_\perp(\mathbf{r},\mathbf{r};\bar{\omega}) + G_\parallel(\mathbf{r},\mathbf{r};\bar{\omega})\right] = \frac{1}{2}(\Gamma_\perp + \Gamma_\parallel), \tag{10}$$

$$\kappa = \frac{\mu_0 \mu^2 \bar{\omega}^2}{2\hbar}\, Im\left[G_\perp(\mathbf{r},\mathbf{r};\bar{\omega}) - G_\parallel(\mathbf{r},\mathbf{r};\bar{\omega})\right] = \frac{1}{2}(\Gamma_\perp - \Gamma_\parallel), \tag{11}$$

$G_\perp(\mathbf{r},\mathbf{r};\bar{\omega}) = G_{zz}(\mathbf{r},\mathbf{r};\bar{\omega})$ and $G_\parallel(\mathbf{r},\mathbf{r};\bar{\omega}) = G_{xx}(\mathbf{r},\mathbf{r};\bar{\omega})$ denote the components of the Green's tensor, where $\perp(\parallel)$ corresponds to a dipole oriented normal, along the z axis (parallel, along the x axis) to the plane of the 2D plasmonic metasurface. The spontaneous-emission rates for a dipole oriented normal and parallel to the metasurface are given by $\Gamma_{\perp,\parallel} = \mu_0 \mu^2 \bar{\omega}^2\, Im\left[G_{\perp,\parallel}(\mathbf{r},\mathbf{r};\bar{\omega})\right]/\hbar$. The degree of quantum interference is provided by

$$p = (\Gamma_\perp - \Gamma_\parallel)/(\Gamma_\perp + \Gamma_\parallel). \tag{12}$$

The peak value of quantum interference in spontaneous emission is $p = 1$ [59]. This is possible if we place the quantum emitter close to a surface that possesses a negligible $\Gamma_\perp$. If the quantum emitter lies in free space, $\Gamma_\perp = \Gamma_\parallel$, resulting in $\kappa = 0$ suggesting the complete absence of quantum interference in the emitter.

As a plasmonic metasurface, we take a two-dimensional square lattice of dielectric (silica) spheres coated with gold (plasmonic material) [Figure 1b,c]. Such nanostructures are routinely fabricated by self-assembly [65], nanopatterning and nanolithographic [66,67] techniques. The dielectric function of the shell is described by the free-electron Drude model

$$\epsilon(\omega) = 1 - \frac{\omega_p^2}{\omega(\omega + i/\tau)}. \tag{13}$$

ω_p is the bulk plasma frequency of the metal, whilst τ is the relaxation time of the conduction-band electrons. For gold, the plasma frequency $\hbar\omega_p = 8.99\,eV$ fixing the corresponding length scale of our calculations as $c/\omega_p \approx 22\,nm$. The electric permittivity of SiO_2 is taken to be constant, $\epsilon = 2.1$. In all the calculations that follow, we assumed $\tau^{-1} = 0.05\omega_p$. The square lattice of nanoshells has a period of $a = 2c/\omega_p$, whilst the corresponding radii of the sphere and core are $S = c/\omega_p$ and $S_c = 0.7c/\omega_p$, respectively. Explicit relations that provide the electromagnetic Green's tensor for a two-dimensional lattice of spheres can be found elsewhere [13,68,69].

In the calculations that follow, we take $\bar{\omega} = 0.632\omega_p$. d stands for the distance between the quantum emitter and the surface of the plasmonic metasurface of gold nanoshells. We assumed that the quantum emitter is placed opposite the center of a nanoshell of the metasurface. The spectra of $\Gamma_\perp$ and $\Gamma_\parallel$ were directly taken from Figure 3 in [21], where it was demonstrated that $\Gamma_\parallel$ is suppressed to such degree that it actually becomes significantly lower than the decay rate of the quantum emitter in a vacuum. $\Gamma_\perp$ is a decreasing function of the separation between the quantum emitter and the plasmonic metasurface.

Moreover, when the emitter is located very close to the metasurface, $\Gamma_\perp$ becomes much larger than the decay rate in a vacuum. Namely, for distances up to $0.6c/\omega_p$, $\Gamma_\perp$ assumes much higher values than the corresponding vacuum decay rate. On the other hand,

for distances between $0.65c/\omega_p$ and c/ω_p, $\Gamma_\perp$ becomes smaller than the corresponding free-space decay rate.

2.2. Susceptibility

The electric susceptibility of the quantum system describing the absorption and dispersion properties of the weak probe field is written as

$$\chi(\delta) = \frac{\sqrt{2}N\mu}{\varepsilon_0 E}(\rho_{21} + \rho_{31}) = \frac{N\mu^2}{\varepsilon_0 \hbar}\frac{\rho_{21} + \rho_{31}}{\Omega}, \tag{14}$$

where the steady state of the density matrix Equations (3)–(7) are ρ_{21} and ρ_{31}, while ε_0 and N are the vacuum permittivity and numerical density of the quantum emitters, respectively.

Calling on Equations (3)–(7), it is easy to find

$$\rho_{21} + \rho_{31} = i\frac{\Omega}{2}\frac{[(X+\kappa)(\rho_{33}-\rho_{11}) + (Y+\kappa)(\rho_{22}-\rho_{11})] + [\rho_{32}(\kappa+X) + \rho_{23}(\kappa+Y)]}{qz - \kappa^2}, \tag{15}$$

where $q = \left[i\delta + \frac{i\omega_{32}}{2} - \gamma - r\right]$ and $z = \left[i\delta - \frac{i\omega_{32}}{2} - \gamma - r\right]$. Here, $\rho_{ii}(i=1,2,3)$ shows the steady state population of levels $|j\rangle$, and

$$\rho_{23} = \rho_{32}^* = \frac{\kappa(\rho_{22}+\rho_{33})}{i\omega_{32}-2\gamma}, \tag{16}$$

describes the coherence term induced by quantum interference of spontaneous emission.

One can decompose Equation (15) into two parts. The first term (containing two sub-terms) comes from the direct transitions $|1\rangle \rightarrow |2\rangle$ and $|1\rangle \rightarrow |3\rangle$ and depends on the population inversions $(\rho_{ii} - \rho_{11})$ $(i = 2, 3)$, while the second term is due to quantum interference when the quantum system is placed in the vicinity of the plasmonic nanostructure and is proportional to the coherence terms ρ_{32} and ρ_{23}.

2.3. Optical Bistability in a Unidirectional Ring Cavity

To characterize the OB features, we consider a medium of length L described by the permittivity of Equation (14) embedded in a unidirectional ring cavity, as illustrated in Figure 1d. The mirrors 3 and 4 are taken as perfect reflectors. The corresponding reflection and transmission coefficients of mirrors 1 and 2 are given by R and T, respectively, with $R + T = 1$. For a perfectly tuned cavity and in the steady-state limit, the boundary conditions between the incident field E^I and the transmitted field E^T read as [70]

$$E(L) = E^T/\sqrt{T}, \tag{17}$$

$$E(0) = \sqrt{T}E^I + RE(L). \tag{18}$$

The second term on the right-hand side of Equation (18) describe the multiple-reflection processes between the mirrors of the cavity, which provides the occurring OB. Clearly, for $R = 0$ in Equation (18), bistability disappears. The boundary conditions and mean-field limit determine the transmitted field in the steady-state,

$$y = 2x - iC(\rho_{21} + \rho_{31}), \tag{19}$$

where $\rho_{21} + \rho_{31}$ is given by Equation (15). $y = \mu E^I/\hbar\sqrt{T}$ and $y = \mu E^T/\hbar\sqrt{T}$ correspond to the normalized input and output fields, respectively. The parameter $C = N\omega L\mu^2/2\hbar\varepsilon_0 cT$ is the cooperative parameter for a system in a ring cavity.

3. Results and Discussion

Next, we calculate the input–output curves for the quantum-sample (emitter + meta-surface) medium immersed in the optical ring cavity and compare them with the case where a medium of solely quantum emitters is placed in the cavity (absence of the plas-

monic metasurface). Namely, in Figure 2, we show the OB in the absence of the incoherent pumping $r = 0$ and for the resonance condition $\delta = 0$. We considered the case of a degenerate system, i.e., $E_2 = E_3$, yielding $\omega_{32} = 0$.

One can see that the OB is already present even in the absence of a plasmonic metasurface (medium of sole quantum emitters) i.e., $d = \infty$ (solid curve). However, by inserting the quantum-sample medium (emitter + plasmonic nanostructure) inside the ring cavity, and for distances $d = 0.7c/\omega_c$ (dot-dashed curve) and $d = 0.9c/\omega_c$ (dashed curve) of the emitter from the metasurface, we observe a significant modification of the area of the hysteresis cycle due to the reduction of the threshold intensity for both the lower and higher branches (the reduction of the higher branch is more dramatic).

The reason for this behavior can be qualitatively interpreted as follows. In the presence of a plasmonic metasurface, very narrow resonances take place at the zero detuning of probe absorption profile (not shown here). In this case, the whole of the absorption spectra is enhanced as $\Gamma_\perp$ and $\Gamma_\parallel$ decrease with distance. Moreover, the width of the absorption peaks are also reduced with $\Gamma_\perp$, leading to very sharp resonant absorption peaks, which may result in a reduction in the threshold intensities for both the lower and upper branches of the OB profile.
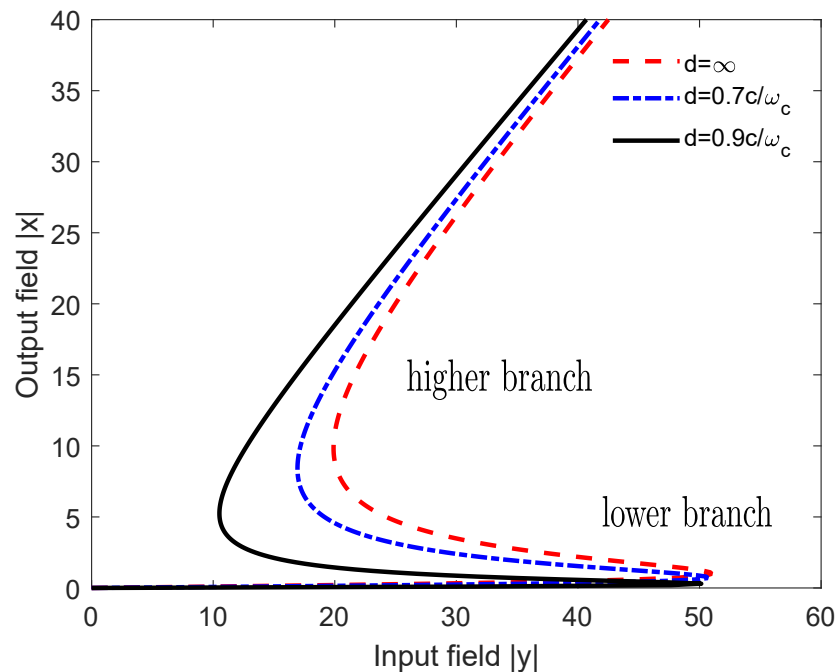

Figure 2. Plots of the input–output field curves for the quantum *V*-system. The dashed curve corresponds to the case of a medium of sole quantum emitters, i.e., $d = \infty$, in which case, the decay rate is Γ_0. The dot-dashed ($d = 0.7c/\omega_c$) and solid ($d = 0.9c/\omega_c$) curves correspond a quantum-sample medium (emitter + metasurface) with $\bar{\omega} = 0.632\omega_p$. We assumed that $\omega_{32} = 0, r = 0, C = 100$ and $\delta = 0$.

The OB features change drastically when we consider a degenerate system ($\omega_{32} \neq 0$). In Figure 3, we show the scaled feedback output field versus the scaled input field for $\omega_{32} = \Gamma_0$ and $r = 0$ and for different values of probe-field detuning. We have assumed that the the *V*-type quantum emitter in the quantum sample is located at distance $d = 0.8c/\omega_c$ from the plasmonic metasurface. It is clear that no OB can be realized on resonance ($\delta = 0$) with the probe field (solid curve).

By slightly increasing the probe-field detuning to $\delta = 0.1\Gamma_0$ (see the dotted curve), the hysteresis cycle appears, giving rise to the optical bistability. A further increase of δ leads the hysteresis cycle to become larger continually with a subsequent increase in the threshold intensity of OB in both the lower and higher branches. Physically, an induced

transparency (zero absorption) will occur on resonance ($\delta = 0$) with the energy absorption spectra of the quantum *V*-system, leading to a perfect transmission of the probe laser field.

The slope of dispersion will be positive around the zero detuning, with an exact zero value for the dispersion and optical Kerr nonlinearity at $\delta = 0$, leading to no OB features. However, away from zero detuning, absorption, dispersion and Kerr nonlinear effects emerge—namely, there is a significant increase in the probe absorption for larger detunings (not shown here) for which the cavity field can hardly achieve saturation, leading to a subsequent enhancement in the OB threshold intensity.
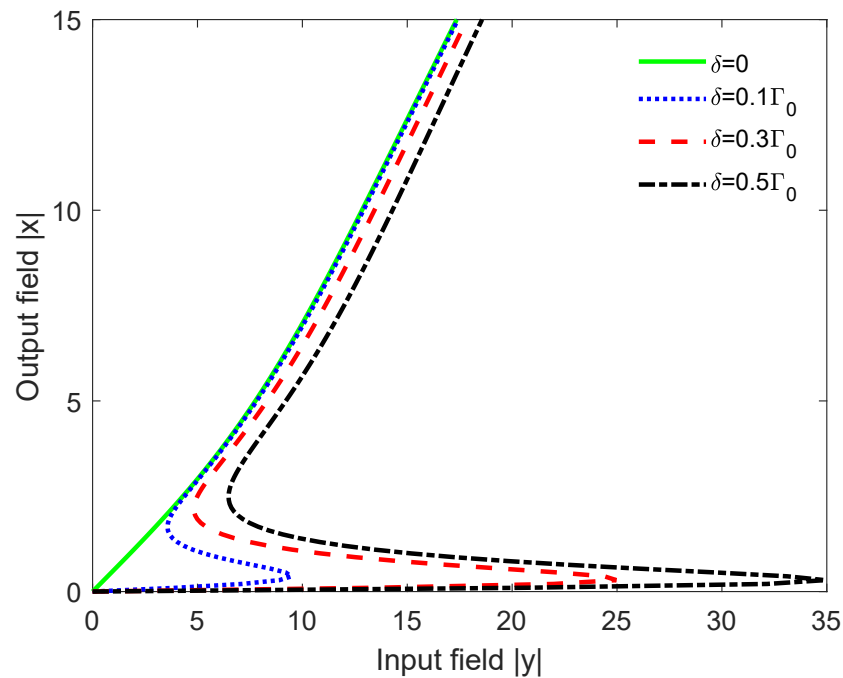
Figure 3. Plots of the input–output field curves for the quantum sample (emitter + metasurface) for different values of emitter-metasurface distance δ. We take $\bar{\omega} = 0.632\omega_p$, $\omega_{32} = \Gamma_0$, $r = 0$, $C = 100$ and $d = 0.8c/\omega_c$.

In Figure 4, we show the effect of distance d from the plasmonic metasurface on the behavior of OB for $\delta = 0.35\Gamma_0$, $\omega_{32} = 0.25\Gamma_0$, and $r = 0$. We observe that, by varying the distance from $d = 0.3c/\omega_c$ (dot-dashed curve) to $d = 0.5c/\omega_c$ (solid curve), we have a transition from OB to OM with a significant reduction in the OM threshold intensity. Realization of OM in quantum systems near plasmonic nanostructures might find application in all-optical switching or coding elements.

One can see that in this case, there are two S-shaped curves for a certain input intensity domain in the input–output solution. When the input field power is increased from zero, the output intensity of the cavity remains on the lower branch. As soon as the output intensity approaches to the threshold of the onset of first S-shaped curve (lower branch), it jumps up to the middle branch, and, from there, again jumps up to a higher branch (tristability). The OB appears again for the larger distance $d = 0.7c/\omega_c$ (dashed curve). The OB threshold increases again and becomes larger than the OM threshold intensity.
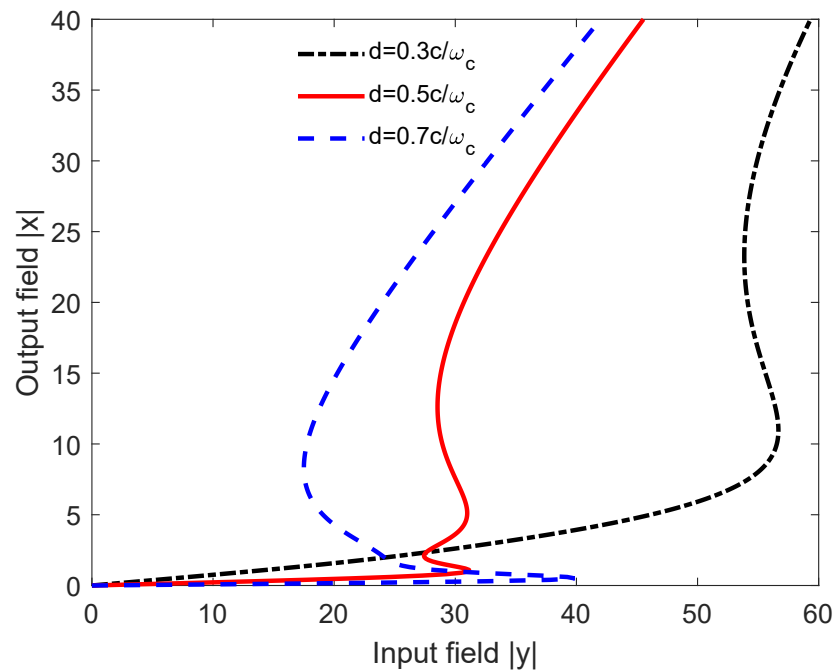
Figure 4. Plots of the input–output field curves for the quantum sample (emitter + metasurface) for different distances d of the emitter from the plasmonic metasurface. We take $\bar{\omega} = 0.632\omega_p$, $\omega_{32} = 0.25\Gamma_0$, $r = 0$, $C = 100$ and $\delta = 0.35\Gamma_0$.

The effect of the incoherent pumping rate r on the OB spectra of the quantum sample is shown in Figure 5, for $d = 0.8c/\omega_c$ and for $\omega_{32} = \Gamma_0$. Interestingly, the threshold of OB first decreases by increasing the rate of the incoherent pumping field (Figure 5a). For stronger incoherent pumping rates, the threshold of the OB starts to increase by increasing the rate of the incoherent pumping field, as can be seen in Figure 5b,c.
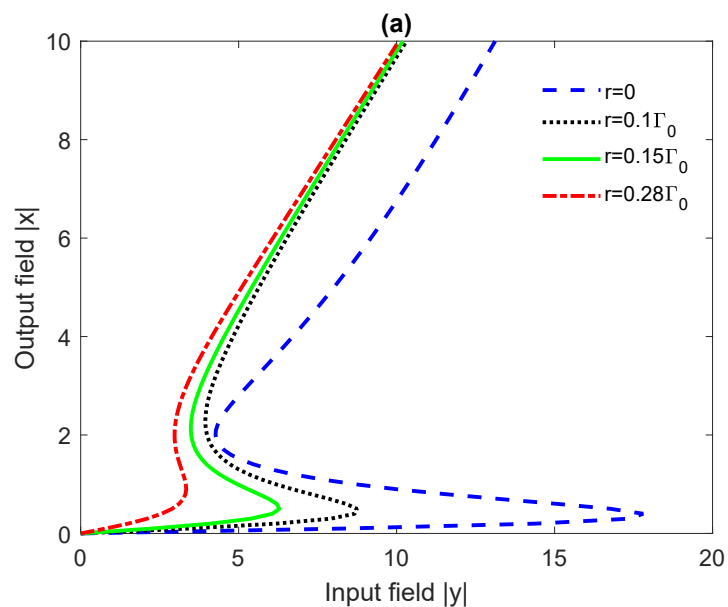

Figure 5. *Cont.*
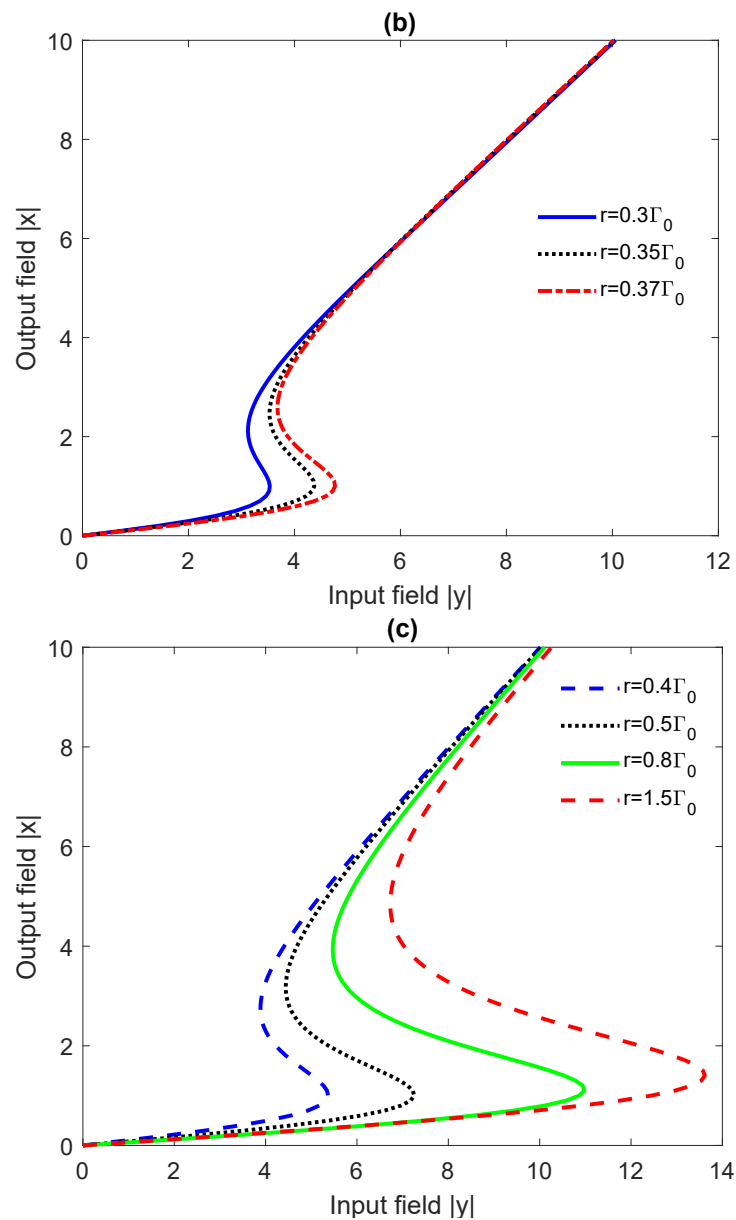
Figure 5. Plots of the input–output field curves for the quantum sample (emitter + metasurface) for various values of the distance d. In (**a**), the incoherent pumping rate r varies from 0 to $0.28\Gamma_0$; in (**b**), from $0,3\Gamma_0$ to $0.37\Gamma_0$; and, in (**c**), from $0,4\Gamma_0$ to $1.5\Gamma_0$. We take $\bar{\omega} = 0.632\omega_p$, $\omega_{32} = \Gamma_0$, $C = 100$ and $\delta = 0.2\Gamma_0$ and $d = 0.8c/\omega_c$.

In Figure 6a, we show the population distributions ρ_{11}, ρ_{22} and ρ_{33}, and (b) and the lasing spectrum $[Im(\chi)]$ of the probe field versus the incoherent pumping. Here, the most interesting result relies on the creation of three different regimes for the incoherent pumping to create OB. The first regime is for the incoherent pumping $r < r_T^L$ where the system is absorptive and no population inversion exists (red zone in Figure 6b).

The observed OB in Figure 5a can be attributed to the presence of absorption in the medium. The second regime is $r_T^L < r < r_T^{PI}$ where gain without population inversion takes place (green zone in Figure 6b). The OB in Figure 5b can be attributed to such a gain without inversion. Lastly, there is a regime with $r > r_T^{PI}$ where the gain is with population inversion (blue zone in Figure 6b), which is responsible for the creation of OB spectra illustrated in Figure 5c.

In the first regime where the incoherent pumping rate is very weak (r from 0 to $r_T^L = 0.28\Gamma_0$), the absorption decreases by increasing the rate of incoherent pumping field.

The reduction in the probe absorption may enhance the Kerr nonlinearity of the quantum system, allowing for direct saturation of the cavity field. This yields a reduction of the OB threshold intensity as observed in Figure 5a.

On the other hand, the coherence between upper states will be destroyed by the stronger incoherent pumping from the lower level to the upper levels ($r > r_T^L$) as the gain starts emerging in the system. The enhancement of the probe gain increases the difficulty of the cavity field to reach saturation, resulting in an increase in the OB threshold intensity (as observed in Figure 5b,c).

We should point out that the presence of a plasmonic metasurface makes it almost impossible to determine analytically a limit for the gain r_T^L as, in this case, the analytical solutions are quite long, complicated and non-informative. We, therefore, used the numerical results to identify the limits for the lasing threshold r_T^L. However, we present analytically the limit for the incoherent pumping to make population inversion in the system. Calling on Equations (5)–(7), one can obtain expressions for the population inversion as

$$\rho_{22} - \rho_{11} = \rho_{33} - \rho_{11} = \left(\frac{r}{2\gamma - \frac{8\gamma\kappa^2}{4\gamma^2 + \omega_{32}^2}} - 1 \right) \rho_{11}. \tag{20}$$

Equation (20) shows that the population differences $\rho_{22} - \rho_{11}$ and $\rho_{33} - \rho_{11}$ depend on the incoherent pumping rate r as well as the quantum interference determined by κ, which is varying by the distance from the plasmonic nanostructure. Plugging equations Equations (10) and (11) into Equation (20), the limit for the incoherent pumping to achieve the population inversion can be expressed as

$$r_T^{PI} = (\Gamma_\perp + \Gamma_\parallel) \left[1 - \frac{\Gamma_\perp^2 + \Gamma_\parallel^2 - 2\Gamma_\perp\Gamma_\parallel}{\Gamma_\perp^2 + \Gamma_\parallel^2 + 2\Gamma_\perp\Gamma_\parallel + \omega_{32}^2} \right]. \tag{21}$$

Clearly, the population inversion is dominant if $r_T^{PI} > (\Gamma_\perp + \Gamma_\parallel) - \frac{(\Gamma_\perp + \Gamma_\parallel)\left(\Gamma_\perp^2 + \Gamma_\parallel^2 - 2\Gamma_\perp\Gamma_\parallel\right)}{\Gamma_\perp^2 + \Gamma_\parallel^2 + 2\Gamma_\perp\Gamma_\parallel + \omega_{32}^2}$, otherwise no inversion appears in the population distributions. These effects are illustrated in Figure 6a.
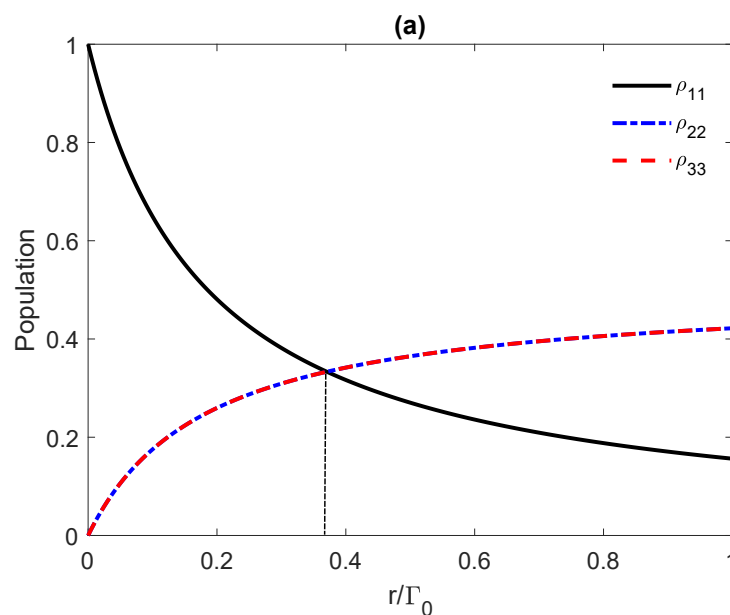

Figure 6. *Cont.*
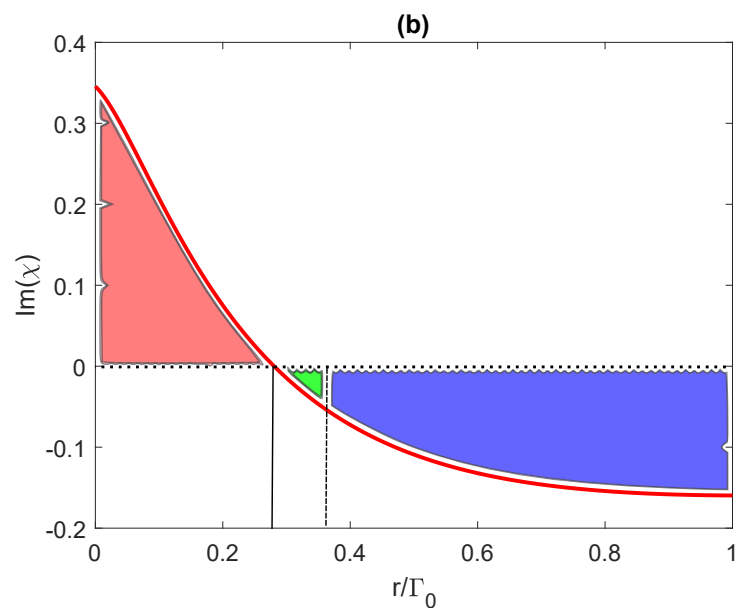
Figure 6. (**a**) The population distributions ρ_{11}, ρ_{22} and ρ_{33}, (**b**) and the gain spectrum $[Im(\chi)]$ (in units of $\frac{N\mu^2}{\varepsilon_0\hbar}$) of the quantum *V*-system as a function of the incoherent pumping *r* in the presence of a plasmonic nanostructure. We take here $\omega_{32} = 0.25\Gamma_0$, and $\delta = 0.2\Gamma_0$ and $d = 0.8c/\omega_c$. The horizontal dotted line indicates the zero absorption limit, while the vertical dashed (solid) line indicates the limit for the incoherent pumping to achieve the population inversion r_T^{PI} (gain r_T^L). Absorption takes place in $r < r_T^L$ (the red zone in (**b**)). Gain without inversion appears in $r_T^L < r < r_T^{PI}$ (the green zone in (**b**)), while the lasing with inversion takes place when $r > r_T^{PI}$ (the blue zone in (**b**)).

4. Conclusions

In conclusion, we demonstrated, theoretically, that it is possible to achieve a controllable shift of the OB threshold intensity as well as modification of the hysteresis curve of OB for a quantum sample placed within an optical ring cavity where, for a quantum sample, we referred to a V-type quantum emitter coupled with a plasmonic metasurface. These unique features of the OB are a result of the enormous enhancement of the quantum interference in the quantum emitter imparted by the presence of the plasmonic metasurface, which, in our case, was a square lattice of gold-coated silica nanospheres (a lattice of plasmonic nanoshells).

The effect of different system parameters on the OB were also studied. We found, in particular, that the OB could be switched to OM by varying the distance of the quantum emitter from the plasmonic metasurface. When the quantum system was pumped by an one-way incoherent pumping field, the bistability could appear with absorption and gain, with or without population inversion. The results may find technological application in the realization of more efficient all-optical switches and logic-gate devices for optical computing and quantum information processing.

Author Contributions: Writing—original draft, H.R.H.; Writing—review and editing, E.P. and V.Y. All authors have read and agreed to the published version of the manuscript.

Data Availability Statement: Data are available from the authors on request.

Conflicts of Interest: The authors declare no conflict of interest.

References

1. Gibbs, H.M.; McCall, S.L.; Venkatesan, T.N.C. Differential Gain and Bistability Using a Sodium-Filled Fabry-Perot Interferometer. *Phys. Rev. Lett.* **1976**, *36*, 1135. [CrossRef]

2. Rosenberger, A.T.; Orozco, L.A.; Kimble, H.J. Observation of absorptive bistability with two-level atoms in a ring cavity. *Phys. Rev. A* **1983**, *28*, 2569. [CrossRef]
3. Harshawardhan, W.; Agarwal, G.S. Controlling optical bistability using electromagnetic-field-induced transparency and quantum interferences. *Phys. Rev. A* **1996**, *53*, 1812. [CrossRef] [PubMed]
4. Chang, H.; Wu, H.; Xie, C.; Wang, H. Controlled Shift of Optical Bistability Hysteresis Curve and Storage of Optical Signals in a Four-Level Atomic System. *Phys. Rev. Lett.* **2004**, *93*, 213901. [CrossRef] [PubMed]
5. Cheng, D.C.; Liu, C.P.; Gong, S.Q. Optical bistability via amplitude and phase control of a microwave field. *Opt. Commun.* **2006**, *263*, 111. [CrossRef]
6. Cheng, D.C.; Liu, C.P.; Gong, S.Q. Optical bistability and multistability via the effect of spontaneously generated coherence in a three-level ladder-type atomic system. *Phys. Lett. A* **2004**, *332*, 244. [CrossRef]
7. Li, J.-H. Controllable optical bistability in a four-subband semiconductor quantum well system. *Phys. Rev. B.* **2007**, *75*, 155329. [CrossRef]
8. Wang, Z.; Xu, M. Control of the switch between optical multistability and bistability in three-level V-type atoms. *Opt. Commun.* **2009**, *282*, 1574. [CrossRef]
9. Sahrai, M.; Asadpour, S.; Sadighi-Bonabi, R. Optical bistability via quantum interference from incoherent pumping and spontaneous emission. *J. Lumin.* **2011**, *131*, 2395. [CrossRef]
10. Hamedi, H.R.; Khaledi-Nasab, A.; Raheli, A.; Sahrai, M. Coherent control of optical bistability and multistability via double dark resonances (DDRs). *Opt. Commun.* **2014**, *312*, 117. [CrossRef]
11. Hamedi, H.R.; Sahrai, M.; Khoshsima, H.; Juzeliunas, G. Optical bistability forming due to a Rydberg state. *J. Opt. Soc. Am. B* **2017**, *34*, 1923. [CrossRef]
12. Fleischhauer, M.; Imamoglu, A.; Marangos, J.P. Electromagnetically induced transparency: Optics in coherent media. *Rev. Mod. Phys.* **2005**, *77*, 633. [CrossRef]
13. Yannopapas, V.; Paspalakis, E.; Vitanov, N.V. Plasmon-Induced Enhancement of Quantum Interference near Metallic Nanostructures. *Phys. Rev. Lett.* **2009**, *103*, 063602. [CrossRef] [PubMed]
14. Evangelou, S.; Yannopapas, V.; Paspalakis, E. Simulating quantum interference in spontaneous decay near plasmonic nanostructures: Population dynamics. *Phys. Rev. A* **2011**, *83*, 055805. [CrossRef]
15. Evangelou, S.; Yannopapas, V.; Paspalakis, E. Modifying free-space spontaneous emission near a plasmonic nanostructure. *Phys. Rev. A* **2011**, *83*, 023819. [CrossRef]
16. Gu, Y.; Wang, L.; Ren, P.; Zhang, J.; Zhang, T.; Martin, O.J.F.; Gong, Q. Polarized linewidth-controllable double-trapping electromagnetically induced transparency spectra in a resonant plasmon nanocavity. *Nano Lett.* **2012**, *12*, 2488. [CrossRef] [PubMed]
17. Artuso, R.D.; Bryant, G.W. Strongly coupled quantum dot-metal nanoparticle systems: Exciton-induced transparency, discontinuous response, and suppression as driven quantum oscillator effects. *Phys. Rev. B* **2010**, *82*, 195419. [CrossRef]
18. Zhang, W.; Govorov, A.O.; Bryant, G.W. Semiconductor-Metal Nanoparticle Molecules: Hybrid Excitons and the Nonlinear Fano Effect. *Phys. Rev. Lett.* **2006**, *97*, 146804. [CrossRef]
19. Singh, M.R.; Schindel, D.G.; Hatef, A. Dipole-dipole interaction in a quantum dot and metallic nanorod hybrid system. *Appl. Phys. Lett.* **2011**, *99*, 181106. [CrossRef]
20. Kosionis, S.G.; Terzis, A.F.; Yannopapas, V.; Paspalakis, E. Nonlocal Effects in Energy Absorption of Coupled Quantum Dot–Metal Nanoparticle Systems. *J. Phys. Chem. C* **2012**, *116*, 23663. [CrossRef]
21. Evangelou, S.; Yannopapas, V.; Paspalakis, E. Transparency and slow light in a four-level quantum system near a plasmonic nanostructure. *Phys. Rev. A* **2012**, *86*, 053811. [CrossRef]
22. Paspalakis, E.; Evangelou, S.; Yannopapas, V.; Terzis, A.F. Phase-dependent optical effects in a four-level quantum system near a plasmonic nanostructure. *Phys. Rev. A* **2013**, *88*, 053832. [CrossRef]
23. Wang, L.; Gu, Y.; Chen, H.; Zhang, J.-Y.; Cui, Y.; Gerardot, B.; Gong, Q.-H. Polarized linewidth-controllable double-trapping electromagnetically induced transparency spectra in a resonant plasmon nanocavity. *Sci. Rep.* **2013**, *3*, 2879. [CrossRef]
24. Wang, Z.-P.; Yu, B.-L. Plasmonic Control of Refractive Index Without Absorption in Metallic Photonic Crystals Doped with Quantum Dots. *Plasmonics* **2018**, *13*, 567. [CrossRef]
25. Evangelou, S.; Yannopapas, V.; Paspalakis, E. Modification of Kerr nonlinearity in a four-level quantum system near a plasmonic nanostructure. *J. Mod. Optic.* **2014**, *61*, 1458. [CrossRef]
26. Chen, H.; Ren, J.; Gu, Y.; Zhao, D.; Zhang, J.; Gong, Q. Nanoscale Kerr Nonlinearity Enhancement Using Spontaneously Generated Coherence in Plasmonic Nanocavity. *Sci. Rep.* **2016**, *5*, 18315. [CrossRef]
27. Hamedi, H.R.; Yannopapas, V.; Mekys, A.; Paspalakis, E. Control of Kerr nonlinearity in a four-level quantum system near a plasmonic nanostructure. *Phys. E Low-Dimens. Syst. Nanostruct.* **2021**, *130*, 114662. [CrossRef]
28. Kosionis, S.G.; Paspalakis, E. Control of Self-Kerr Nonlinearity in a Driven Coupled Semiconductor Quantum Dot–Metal Nanoparticle Structure. *J. Phys. Chem. C* **2019**, *123*, 7308. [CrossRef]
29. Singh, S.K.; Abak, M.K.; Tasgin, M.E. Enhancement of four-wave mixing via interference of multiple plasmonic conversion paths. *Phys. Rev. B* **2016**, *93*, 035410. [CrossRef]
30. Paspalakis, E.; Evangelou, S.; Kosionis, S.G.; Terzis, A.F. Strongly modified four-wave mixing in a coupled semiconductor quantum dot-metal nanoparticle system. *J. Appl. Phys.* **2014**, *115*, 083106. [CrossRef]

31. Sadeghi, S.M. Gain without inversion in hybrid quantum dot–metallic nanoparticle systems. *Nanotechnology* **2010**, *21*, 455401. [CrossRef] [PubMed]

32. Kosionis, S.G.; Terzis, A.F.; Sadeghi, S.M.; Paspalakis, E. Optical response of a quantum dot-metal nanoparticle hybrid interacting with a weak probe field. *J. Phys. Condens. Matter* **2013**, *25*, 045304. [CrossRef]

33. Sadeghi, S.M. Ultrafast plasmonic field oscillations and optics of molecular resonances caused by coherent exciton-plasmon coupling. *Phys. Rev. A* **2013**, *88*, 013831. [CrossRef]

34. Zhao, D.; Gu, Y.; Wu, J.; Zhang, J.; Zhang, T.; Gerardot, B.D.; Gong, Q. Quantum-dot gain without inversion: Effects of dark plasmon-exciton hybridization. *Phys. Rev. B* **2014**, *89*, 245433. [CrossRef]

35. Carreño, F.; Antón, M.A.; Yannopapas, V.; Paspalakis, E. Control of the absorption of a four-level quantum system near a plasmonic nanostructure. *Phys. Rev. B* **2017**, *95*, 195410. [CrossRef]

36. Kosionis, S.G.; Paspalakis, E. Pump-probe optical response of semiconductor quantum dot–metal nanoparticle hybrids. *J. Appl. Phys.* **2018**, *124*, 223104. [CrossRef]

37. Malyshev, A.V.; Malyshev, V.A. Optical bistability and hysteresis of a hybrid metal-semiconductor nanodimer. *Phys. Rev. B* **2011**, *84*, 035314. [CrossRef]

38. Nugroho, B.S.; Malyshev, V.A.; Knoester, J. Tailoring optical response of a hybrid comprising a quantum dimer emitter strongly coupled to a metallic nanoparticle. *Phys. Rev. B* **2015**, *92*, 165432. [CrossRef]

39. Carreno, F.; Anton, M.A.; Paspalakis, E. Nonlinear optical rectification and optical bistability in a coupled asymmetric quantum dot-metal nanoparticle hybrid. *J. Appl. Phys.* **2018**, *124*, 113107. [CrossRef]

40. Nugroho, B.S.; Iskandar, A.A.; Malyshev, V.A.; Knoester, J. Bistable optical response of a nanoparticle heterodimer: Mechanism, phase diagram, and switching time. *J. Chem. Phys.* **2013**, *139*, 014303. [CrossRef] [PubMed]

41. Mohammadzadeh, A.; Miri, M. Optical response of hybrid semiconductor quantum dot-metal nanoparticle system: Beyond the dipole approximation. *J. Appl. Phys.* **2018**, *123*, 043111. [CrossRef]

42. Li, J.-B.; Kim, N.-C.; Cheng, M.-T.; Zhou, L.; Hao, Z.-H.; Wang, Q.-Q. Optical bistability and nonlinearity of coherently coupled exciton-plasmon systems. *Optic Express* **2012**, *20*, 1856. [CrossRef]

43. Nugroho, B.S.; Iskandar, A.A.; Malyshev, V.A.; Knoester, J. Plasmon-assisted two-photon absorption in a semiconductor quantum dot–metallic nanoshell composite. *Phys. Rev. B* **2020**, *102*, 045405. [CrossRef]

44. Tan, Y.; Xia, X.S.; Liao, X.L.; Li, J.B.; Zhong, H.H.; Liang, S.; Xiao, S.; Liu, L.H.; Luo, J.H.; He, M.D.; et al. A highly-flexible bistable switch based on a suspended monolayer Z-shaped graphene nanoribbon nanoresonator. *Carbon* **2020**, *157*, 724. [CrossRef]

45. Li, J.B.; Liang, S.; Xiao, S.; He, M.D.; Kim, N.C.; Chen, L.Q.; Wu, G.H.; Peng, Y.X.; Luo, X.Y.; Guo, Z.P. Four-wave mixing signal enhancement and optical bistability of a hybrid metal nanoparticle-quantum dot molecule in a nanomechanical resonator. *Opt. Express* **2016**, *24*, 2360. [CrossRef]

46. Asadpour, S.H.; Soleimani, H. Optical bistability and multistability in a four-level quantum system in the presence of plasmonic nanostructure. *Phys. E-Low-Dimens. Syst. Nanostruct.* **2016**, *75*, 112. [CrossRef]

47. Solookinejad, G.; Jabbari, M.; Nafar, M.; Ahmadi, E.; Asadpour, S.H. Incoherent control of optical bistability and multistability in a hybrid system: Metallic nanoparticle-quantum dot nanostructure. *J. Appl. Phys.* **2018**, *124*, 063102. [CrossRef]

48. Tohari, M.M.; Alqahtani, M.M.; Lyras, A. Optical Multistability in the Metal Nanoparticle–Graphene Nanodisk–Quantum Dot Hybrid Systems. *Nanomaterials* **2020**, *10*, 1687. [CrossRef]

49. Tohari, M.M. Terahertz Optical Bistability in the Metal Nanoparticles-Graphene Nanodisks-Quantum Dots Hybrid Systems. *Nanomaterials* **2020**, *10*, 2173. [CrossRef]

50. Evangelou, S. Tailoring second-order nonlinear optical effects in coupled quantum dot-metallic nanosphere structures using the Purcell effect. *Microelectron. Eng.* **2019**, *215*, 111019. [CrossRef]

51. Singh, M.R. Enhancement of the second-harmonic generation in a quantum dot–metallic nanoparticle hybrid system. *Nanotechnology* **2014**, *24*, 125701. [CrossRef] [PubMed]

52. Jha, P.K.; Wang, Y.; Ren, X.; Zhang, X. Quantum-coherence-enhanced transient surface plasmon lasing. *J. Opt.* **2017**, *19*, 054002. [CrossRef]

53. Xu, X.; Broussier, A.; Ritacco, T.; Nahra, M.; Geoffray, F.; Issa, A.; Jradi, S.; Bachelot, R.; Couteau, C.; Blaize, S. Towards the integration of nanoemitters by direct laser writing on optical glass waveguides. *Phot. Res.* **2020**, *8*, 1541. [CrossRef]

54. Ge, D.; Marguet, S.; Issa, A.; Jradi, S.; Nguyen, T.H.; Nahra, M.; Béal, J.; Deturche, R.; Chen, H.; Blaize, S.; et al. Hybrid plasmonic nano-emitters with controlled single quantum emitter positioning on the local excitation field. *Nat. Commun.* **2020**, *11*, 3414. [CrossRef] [PubMed]

55. Lio, G.E.; Madrigal, J.B.; Xu, X.; Peng, Y.; Pierini, S.; Couteau, C.; Jradi, S.; Bachelot, R.; Caputo, R.; Blaize, S. Integration of Nanoemitters onto Photonic Structures by Guided Evanescent-Wave Nano-Photopolymerization. *J. Phys. Chem. C* **2019**, *123*, 14669. [CrossRef]

56. Lio, G.E.; Ferraro, A.; Ritacco, T.; Aceti, D.M.; De Luca, A.; Giocondo, M.; Caputo, R. Leveraging on ENZ Metamaterials to Achieve 2D and 3D Hyper-Resolution in Two-Photon Direct Laser Writing. *Adv. Mater.* **2021**, *33*, 202008644. [CrossRef]

57. Fofang, N.T.; Grady, N.K.; Fan, Z.; Govorov, A.O.; Halas, N.J. Plexciton Dynamics: Exciton—Plasmon Coupling in a J-Aggregate—Au Nanoshell Complex Provides a Mechanism for Nonlinearity. *Nano Lett.* **2011**, *11*, 1556. [CrossRef]

58. Agarwal, G.S. Anisotropic Vacuum-Induced Interference in Decay Channels. *Phys. Rev. Lett.* **2000**, *84*, 5500. [CrossRef]

59. Kiffner, M.; Macovei, M.; Evers, J.; Keitel, C.H. Chapter 3—Vacuum-Induced Processes in Multilevel Atoms. *Prog. Opt.* **2010**, *55*, 85.

60. Yang, Y.; Xu, J.; Chen, H.; Zhu, S. Quantum Interference Enhancement with Left-Handed Materials. *Phys. Rev. Lett.* **2008**, *100*, 043601. [CrossRef]

61. Li, G.X.; Evers, J.; Keitel, C.H. Spontaneous emission interference in negative-refractive-index waveguides. *Phys. Rev. B* **2009**, *80*, 045102. [CrossRef]

62. Jha, P.K.; Ni, X.; Wu, C.; Wang, Y.; Zhang, X. Metasurface-Enabled Remote Quantum Interference. *Phys. Rev. Lett.* **2015**, *115*, 025501. [CrossRef]

63. Hughes, S.; Agarwal, G.S. Anisotropy-Induced Quantum Interference and Population Trapping between Orthogonal Quantum Dot Exciton States in Semiconductor Cavity Systems. *Phys. Rev. Lett.* **2017**, *118*, 063601. [CrossRef] [PubMed]

64. Karanikolas, V.; Paspalakis, E. Plasmon-Induced Quantum Interference near Carbon Nanostructures. *J. Phys. Chem. C* **2018**, *122*, 14788. [CrossRef]

65. Zhang, S.; Ni, W.; Kou, X.; Yeung, M.H.; Sun, L.; Wang, J.; Yan, C. Formation of Gold and Silver Nanoparticle Arrays and Thin Shells on Mesostructured Silica Nanofibers. *Adv. Funct. Mater.* **2007**, *17*, 3258. [CrossRef]

66. Liu, J.; Dong, H.; Li, Y.; Zhan, P.; Zhu, M.; Wang, Z. A Facile Route to Synthesis of Ordered Arrays of Metal Nanoshells with a Controllable Morphology. *Jpn. J. Appl. Phys.* **2006**, *45*, L582. [CrossRef]

67. Yang, S.; Cai, W.; Kong, L.; Lei, Y. Surface Nanometer-Scale Patterning in Realizing Large-Scale Ordered Arrays of Metallic Nanoshells with Well-Defined Structures and Controllable Properties. *Adv. Funct. Mater.* **2010**, *20*, 2527–2533. [CrossRef]

68. Sainidou, R.; Stefanou, N.; Modinos, A. Green's function formalism for phononic crystals. *Phys. Rev. B* **2004**, *69*, 064301. [CrossRef]

69. Yannopapas, V.; Vitanov, N. Electromagnetic Green's tensor and local density of states calculations for collections of spherical scatterers. *Phys. Rev. B* **2007**, *75*, 115124. [CrossRef]

70. Bonifacio, R.; Lugiato, L.A. Optical bistability and cooperative effects in resonance fluorescence. *Phys. Rev. A* **1978**, *18*, 1129. [CrossRef]